

1 **Assessing the virulence of *Cryptococcus neoformans* causing meningitis in HIV infected and**
2 **uninfected patients in Vietnam**

3 Lam Tuan Thanh¹, Dena L. Toffaletti², Jennifer L. Tenor², Charles Giamberardino², Gregory D.
4 Sempowski³, Yohannes Asfaw⁴, Hai Trieu Phan¹, Anh Van Duong¹, Trinh Mai Nguyen¹, Guy E.
5 Thwaites^{1,5}, Philip M. Ashton^{1,5}, Chau Van Vinh Nguyen⁶, Stephen G. Baker⁷, John R. Perfect²,
6 and Jeremy N. Day^{1,5}

7 ¹Oxford University Clinical Research Unit, Wellcome Trust Asia Africa Programme, Ho Chi Minh
8 City, Vietnam

9 ²Division of Infectious Diseases, Department of Medicine and Department of Molecular
10 Genetics and Microbiology, Duke University, North Carolina, USA

11 ³Duke Human Vaccine Institute and Regional Biocontainment Laboratory, Duke University,
12 North Carolina, USA

13 ⁴Division of Laboratory Animal Resources, Duke University, North Carolina, USA

14 ⁵Centre for Tropical Medicine and Global Health, Nuffield Department of Medicine, University
15 of Oxford, Oxford, UK

16 ⁶Hospital for Tropical Diseases, Ho Chi Minh City, Vietnam

17 ⁷Cambridge Institute of Therapeutic immunology and Infectious Disease, Department of
18 Medicine, University of Cambridge, Cambridge, UK

19

20 **Correspondence:** Jeremy Day: jday@oucru.org Tel : (+84 8) 39237954 Fax : (+84 8) 39238904

21

22 **Short title:** Characterizing *Cryptococcus neoformans* from HIV uninfected patients

23

24 **Keywords**

25 Cryptococcal meningitis, *Cryptococcus neoformans*, immunocompetent, HIV, virulence

26 **Abstract**

27 We previously observed a substantial burden of cryptococcal meningitis in Vietnam atypically
28 arising in HIV-uninfected individuals. This disease was associated with a single genotype of
29 *Cryptococcus neoformans* (Sequence Type (ST)5), which was significantly less common in HIV-
30 infected individuals. Aiming to compare the phenotypic characteristics of ST5 and non-ST5 *C.*
31 *neoformans* we selected 30 representative Vietnamese isolates, compared their *in vitro*
32 pathogenic potential and *in vivo* virulence. ST5 and non-ST5 organisms exhibited comparable
33 characteristics with respect to *in vitro* virulence markers including melanin production,
34 replication at 37°C, and growth in cerebrospinal fluid. However, the ST5 isolates had
35 significantly increased variability in cellular and capsular sizing compared with non-ST5
36 organisms ($p < 0.001$). Counter-intuitively, mice infected with ST5 isolates had significantly
37 longer survival with lower fungal burdens at day 7 than non-ST5 isolates. Notably, ST5 isolates
38 induced significantly greater initial inflammatory responses than non-ST5 strains, measured by
39 TNF- α concentrations ($p < 0.001$). Despite being generally less virulent in the mouse model, we
40 hypothesize that the significant within strain variation seen in ST5 isolates in the tested
41 phenotypes may represent an evolutionary advantage enabling adaptation to novel niches
42 including apparently immunocompetent human hosts.

43

44

45

46

47 Introduction

48 Cryptococcal meningitis (CM) is a life-threatening fungal infection caused principally by
49 *Cryptococcus neoformans* and *Cryptococcus gattii*¹⁻³. Despite CM being more common in
50 immunocompromised patients, CM can also arise in apparently immunocompetent patients.
51 Recent figures estimate an annual global CM incidence of 223,100 cases in HIV infected
52 patients, resulting in 181,100 deaths⁴.
53 Generally, *C. gattii* is the most common cause of CM in immunocompetent patients, while *C.*
54 *neoformans* is primarily responsible for disease in immunocompromised patients⁵. When CM
55 associated with *C. neoformans* var. *grubii* occurs in HIV-uninfected individuals, reports often
56 describe patients with an increased susceptibility due to other underlying immunosuppressive
57 conditions^{6,7}. In Vietnam, *C. neoformans* var. *grubii* CM in HIV-uninfected patients accounts for
58 approximately 20% of all CM cases admitted to our hospital in Ho Chi Minh City (HCMC)⁸. We
59 previously reported that the majority of HIV-uninfected CM patients had no identified cause or
60 other medical history suggestive of immunosuppression, and that >80% of HIV-uninfected CM
61 patients were infected by a single genotype of *C. neoformans* var. *grubii*⁹, which we later
62 confirmed to be Sequence Type 5 (ST5).

63
64 Our clinical observations have been replicated in China, where >70% of CM cases from
65 apparently immunocompetent individuals were infected with *C. neoformans*^{10,11}. Again these
66 organisms were latterly identified as genotype ST5^{12,13}. Comparably, ST5 accounted for >80% of
67 HIV-uninfected CM patients in South Korea, although some patients from this location had
68 potentially immunosuppressive conditions¹⁴. This association between a ST and host immune

69 phenotype could be explained by lineage-specific increases in pathogenic potential, fitness in
70 the human host, an unidentified host immune deficit, or a combination of these three factors.
71 Recent high-resolution genomic investigation of the population structure of clinical *C.*
72 *neoformans* var. *grubii* isolates in Vietnam has verified that ST5 and ST4 are genetically distinct
73 lineages of *C. neoformans* var. *grubii*, namely VNla-5 and VNla-4¹⁵.

74
75 Here, in order to explore the hypothesis that *C. neoformans* var. *grubii* ST5 have an increased
76 pathogenic potential in comparison to non-ST5 organisms, we compared their *in vitro* virulence
77 phenotypes and exploited an established cryptococcosis mouse model to compare their relative
78 pathogenicity and ability to induce systemic inflammation.

79

80 **Materials and methods**

81 *C. neoformans* isolates and culture conditions

82 We used clinical isolates obtained at the point of diagnosis, prior to antifungal therapy, from
83 the cerebrospinal fluid (CSF) of patients enrolled in a prospective descriptive study of HIV-
84 uninfected patients with central nervous system (CNS) infections, and a randomized controlled
85 trial of antifungal therapy in HIV-infected patients^{8,16}. We randomly selected 15 isolates from
86 HIV uninfected CM patients and 15 from HIV-infected CM patients. MLST profiles (CAP59,
87 GPD1, IGS1, LAC1, PLB1, SOD1, URA5) for all isolates were previously determined¹⁷. *C.*
88 *neoformans* yeasts were propagated using Yeast Peptone Dextrose (YPD) broth and incubated
89 overnight at 30°C with agitation. Isolates and clinical information from corresponding patients
90 are summarized in Table 1.

91
92 *Growth at high temperature, in ex vivo human CSF and melanin production*
93 Growth at high temperature and in *ex vivo* human CSF were tested as previously described¹⁸
94 with modifications for quantitative assessment. To assess fungal growth at different
95 temperatures, the inoculum was adjusted to 10⁸ cells/ml, serially diluted and spot-inoculated in
96 duplicate on YPD agar in 5µl aliquots and incubated at 30°C or 37°C for 48 hours. After 48
97 hours, colony forming units (CFU) were counted and recorded in CFU/ml.

98
99 For the *ex vivo* CSF growth assay, baseline pre-antifungal treatment CSF supernatant from
100 random de-identified HIV-infected patients enrolled into an antifungal therapy trial was pooled,
101 filtered, and stored at -80°C until use. 10µl of 10⁸ cells/ml yeast suspension was inoculated into
102 90µl of pooled CSF and incubated at 37°C with 5%CO₂. Inoculated CSF was serially diluted and
103 spotted on YPD agar at days 1 and 3 post-inoculation. All experiments were repeated in
104 triplicate. The H99-derived mutant *Δena1*, which lacks a cation-ATPase-transporter resulting in
105 decreased viability in human CSF and macrophages, was used as a negative control for the *ex*
106 *vivo* CSF assay¹⁹. H99 was included as a reference in all experiments. Data were standardized
107 by expressing the results as a ratio of the CFU/ml of the test isolate to the CFU/ml of H99.
108 Melanin production was assessed by plating 5µl of 10⁶ cells/mL cell suspension on L-DOPA agar
109 containing 1g/L L-asparagine, 1g/L glucose, 3g/L KH₂PO₄, 250mg/L MgSO₄·7H₂O, 1mg/L
110 Thiamine HCl, 5µg/L Biotin, 100mg/L L-DOPA, 20g/L Bacto Agar^{20,21}. Plates were incubated in
111 the dark at 30°C or 37°C for 3 days. Differences in colony melanization were compared visually

112 with reference to H99 and an H99-derived mutant with diminished melanization in L-DOPA
113 agar from the Perfect lab.

114

115 *Extracellular urease and phospholipase activity*

116 Extra-cellular urease production was semi-quantified using Christensen's agar. $10\mu\text{l}$ of 10^8
117 cells/ml yeast suspension was spotted on Christensen's agar and incubated at room
118 temperature. The time to complete plate colouration was determined using a GoPro Hero 6
119 camera (Gopro, USA) using the time-lapse setting set with a 1-minute interval. *C. neoformans*
120 H99 was used as a positive control and *Candida albicans* as a negative control. Extracellular
121 phospholipase activity was screened on egg yolk medium as previously described, with minor
122 modifications²². The egg yolk medium contained Sabouraud agar with 1M sodium chloride,
123 0.005M calcium chloride and 8% sterile egg yolk enrichment (Merck, USA). A $5\mu\text{l}$ aliquot of *C.*
124 *neoformans* yeast suspension (10^8 cells/ml) was spotted on egg yolk agar and incubated at 30°C
125 for 72 hours. The diameters of the precipitation zone (D) formed around the colonies and of the
126 respective colonies (d) were recorded after 72 hours incubation. The D/d ratio for each isolate
127 was calculated. H99 was included for reference in each experimental batch. The final result for
128 each isolate was expressed as the ratio between the test isolate's D/d ratio and that of H99. All
129 isolates were tested in triplicate for each phenotype.

130

131 *In vitro capsule and cell size measurement*

132 To measure *in vitro* cryptococcal capsule thickness, all isolates were streaked onto capsule-
133 inducing agar containing powdered Dulbecco Modified Eagle Medium (DMEM) [supplemented

134 with 4.5g/L glucose, L-glutamine, sodium pyruvate], NaHCO₃ 250mM, NaMOPS 1M, Neomycin
135 200mg/ml, Cefotaxime 100 mg/ml²³. Plates were incubated at 37°C in 5% CO₂ until single
136 colonies were visible. Unless otherwise specified, all reagents were purchased from Sigma-
137 Aldrich. India ink smears from a single yeast colony were prepared on a glass slide and
138 visualized at 100X magnification using a CX41 microscope (Olympus, Japan). Images of single
139 microscopic yeast cells were captured using a DP71 Camera system with DP Controller software
140 (Olympus, Japan) and processed using ImageJ (rsb.info.nih.gov/ij/). Capsular thickness was
141 calculated by subtracting yeast cell body diameter (D_{CD} , no capsule) from whole cell diameter
142 (D_{WC} , including capsule). At least 30 individual microscopic yeast cells were assessed for each
143 isolate.

144

145 *Mouse inhalation infection model of cryptococcosis*

146 All mouse infection experiments were conducted as previously described according to Duke
147 University's Institutional Animal Care and Use Committee guidelines and approvals²⁴. Six-week
148 old female A/J mice were sedated with isoflurane and inoculated intranasally with the selected
149 *C. neoformans* var. *grubii* isolate by dropping 25µl of yeast suspension containing 5×10^4 cells
150 into the nares. Eight isolates were randomly selected from the 30 for murine experiments. The
151 isolates were five ST5 (BK147 and BK44 from HIV infected patients and BMD700, BMD1338 and
152 BMD1646 from HIV uninfected patients) and three non-ST5 strains (BMD1415 (ST4) and
153 BMD1367 (ST306) from HIV uninfected patients and BK80 (ST4) from an HIV infected patient).
154 Animals were monitored daily and euthanized by CO₂ inhalation at indicated time points (fungal

155 burden and *in vivo* responses) or until weight loss \geq 15% body weight was observed (virulence
156 assay).

157

158 *Determining in vivo fungal burden*

159 Five mice were infected with each isolate in two independent experiments for assessment of
160 fungal burden at 7- or 14-days post-infection. All animals in each experiment set were
161 euthanized by CO₂ inhalation either on day 7 or day 14 post-infection. Fungal burden at each
162 time point was assessed by excising the left superior lobe of the lung and brain and
163 homogenizing the tissue by bead beating. Tissue homogenate was serially diluted and plated
164 onto YPD agar supplemented with 100mg/ml ampicillin. The plates were incubated at 30°C for
165 48 hours and the number of *C. neoformans* colony forming units (CFU) recorded. Fungal
166 burdens were expressed as CFU per gram of tissue (CFU/g). At each time point, additional lung
167 lobes were also collected for determining *in vivo* histopathology and cytokine response, as
168 described below. In addition, fungal burdens were separately determined at the point of death
169 in animals from the survival assays described below.

170

171 *Determining in vivo histopathology*

172 At specific time points (7 or 14 days post-infection, as described above), the right superior lung
173 lobe from each mouse was excised and immersed in 10% formalin (replaced with 70% ethanol
174 after 24 hours) for fixation. Fixed, uninflated lung specimens were stored at 4°C until further
175 processing. After paraffin embedding, sliced sections were stained using the periodic acid-Schiff
176 (PAS) or mucicarmine stains. Histopathological examination was performed by an independent

177 pathologist blinded to infecting strain. Tissue damage was scored from 0 (no changes) to 10
178 (severe changes), corresponding to the severity of pathology in 4 different categories: necrosis,
179 hemorrhage, edema and inflammation, as per the Duke Veterinary Diagnostic Laboratory
180 (Division of Laboratory Animal Resources).

181

182 *Determining in vivo cytokine response*

183 To assess the severity of the inflammatory responses at specific time points (day 7 and day 14
184 post-infection), the middle lobe from the right lung of each infected mouse was excised and
185 homogenized by bead beating in 1ml sterile PBS/Protease inhibitor. 500µl of lung homogenate
186 was used for cytokine profiling. Cytokines representing T-helper type 1 (Th1) (IL-12p70, TNF-α,
187 IFN-γ), T-helper type 17 (IL-17) and T-helper type 2 (Th2) (IL-4, IL-5, IL-10) responses were
188 measured using a customized Bio-Plex Pro™ Mouse Cytokine Th1/Th2 Assay kit (Biorad, USA)
189 with the BioPlex 200 platform according to the manufacturer's guidelines. Data were retrieved
190 using BioPlex Manager Software. The upper and lower limits of quantification (ULOQ and LLOQ)
191 were based on a standard curve. All values falling below the LLOQ were replaced with the
192 midpoint between zero and the LLOQ. Data were standardized by lung weight and presented as
193 picogram of cytokines per gram lung tissue (pg/g).

194

195 *In vivo virulence assay*

196 The virulence assay was conducted independently from the day 7/day 14 experiment. Each of
197 the 8 selected isolates was inoculated intranasally into 10 A/J mice. Mice were monitored daily

198 until death, or loss of more than 15% body weight (impending death), at which point they were
199 euthanized by CO₂ inhalation, necropsied and had fungal burden in lung and brain determined.

200

201 *Statistical analysis*

202 GraphPad Prism version 5.04 for Windows (GraphPad Software, San Diego California USA;
203 www.graphpad.com) was used for data visualization and statistical analyses of fungal loads,
204 cytokine profiling, capsular/cell size, and survival proportions. The Mann-Whitney U-test was
205 used for comparing fungal load and cytokine concentrations. Kaplan-Meier survival curves and
206 the log-rank test were used for survival analysis. Capsule/cell size was compared using Welch's
207 t-test. The Fligner-Killeen test of variance homogeneity for analyzing variation in capsule/cell
208 size and Fisher's exact test were performed using R software, version 3.2.4 ([http://www.r-](http://www.r-project.org)
209 [project.org](http://www.r-project.org)). One way ANOVA with post hoc multiple comparison tests (Dunnett or Bonferroni)
210 was used to compare cytokine concentrations between individual isolates.

211

212 **Results**

213 *C. neoformans in vitro virulence*

214 We compared the capsule size, extracellular urease, phospholipase production, melanin
215 production, growth at high temperature, and growth in pooled human CSF between the 15 ST5
216 and the 15 non-ST5 *C. neoformans* isolates. We observed no significant genotype-specific
217 differences between growth at 30°C ($p=0.10$), growth at 37°C ($p=0.23$), *ex vivo* survival in CSF
218 after 1-day ($p=0.72$), *ex vivo* survival in CSF after 3-days of exposure ($p=0.77$), extracellular
219 urease activity, or phospholipase activity (Figure S1). ST5 *C. neoformans* cells developed

220 significantly thicker capsules during *in vitro* culture than non-ST5 isolates (Table 2). Individual
221 ST5 *C. neoformans* cells were also significantly larger than non-ST5 cells (Figure 1), and we
222 observed significantly greater variation in capsule size and cell diameter within ST5 cells than
223 non-ST5 cells (Figure 1; $p < 0.0001$, Fligner-Killeen test). Notably, a single organism (BMD1646),
224 was clearly larger and with thicker capsules than other isolates. However, the difference in
225 capsule thickness and cell diameter between STs remained statistically significant even when
226 this isolate was removed from analysis.

227

228 *In vivo* mouse infections with ST5 and non-ST5 isolates

229 We hypothesized that a higher prevalence of ST5 infections in apparently healthy hosts was
230 associated with higher virulence. Therefore, we challenged A/J with equivalent doses of
231 representative isolates (5 ST5 and 3 non-ST5; the individual *in vitro* virulence phenotyping
232 results for these 8 isolates are presented in supplementary Figures S2-S4). Contrary to our
233 hypothesis, we found that mice infected with ST5 organisms had significantly longer survival
234 times than mice infected with non-ST5 organisms ($p < 0.0001$, Figure 2A). However, there was
235 significant variability in the effect of individual organisms of the same ST on survival (Figure 2B).
236 Specifically, two ST5 organisms (BK147 and BMD1646) were substantially attenuated in
237 comparison to other ST5 organisms; the mice infected with these organisms survived up to 40
238 days. However, differences in survival times between mice infected with ST5 and non-ST5
239 organisms remained significant when these two isolates were removed from the analysis
240 ($p = 0.003$; log-rank test).

241

242 The tissue-specific fungal burden data are shown in Table 3. All organisms established lung
243 infection and disseminated brain infection as early as 7 days post infection. Non-ST5 infections
244 resulted in higher fungal burdens in lung than ST5 infections at all time-points (day 7, $p<0.001$;
245 day 14, $p<0.0001$; and end of the experiment, $p<0.0001$ (Figure 3). Again, these data were not
246 driven by the two apparently attenuated ST5 isolates as the fungal loads associated with the
247 ST5 infections were significantly lower even when excluded from the analysis. The majority of
248 animals infected with the attenuated ST5 organisms (BMD1646 (4/5 mice) and BK147 (5/5
249 mice)) had low fungal burdens in the lungs up to day 14 (Figure 3). Fungal burdens in the brain
250 were higher in non-ST5 infected animals at all time points; however, this difference was only
251 statistically significant at the end of the experiment ($p=0.054$, $p=0.36$, and $p=0.01$; Mann-
252 Whitney test at days 7, 14 and point of impending death (time when 15% body weight loss is
253 observed).

254

255 *ST5 C. neoformans isolates induce of TNF- α in the lungs of infected mice*

256 We next measured the cytokine concentrations in lung homogenates at days 7 and 14 post-
257 infection (Figure 4). The concentrations of TNF- α were significantly higher in lung homogenates
258 from mice infected with ST5 than non-ST5 infections ($p=0.01$). Of note, the highest day 7 lung
259 TNF- α concentrations were associated with the ST5 organisms that were most attenuated in
260 the mouse survival model (BK147 and BMD1646). Correspondingly, the lowest TNF- α
261 concentrations were measured in the most virulent ST5 isolate in the mouse model (BMD1338).
262

263 By day 14, the mean TNF- α concentrations in lung homogenates associated with the ST5
264 infections had declined from 3933.71 pg/g lung to 2802.36 pg/g lung ($p < 0.001$). Other Th-1
265 cytokines including IL-12, IL-17, and IFN- γ also decreased in ST5-infected mice between days 7
266 and 14 ($p < 0.001$, $p < 0.01$ and $p = 0.02$, respectively). This contrasted with the non-ST5 infections,
267 in which the mean TNF- α levels had increased from 3256.25 pg/g to 6378.76 pg/g ($p = 0.02$) over
268 this same period. The high TNF- α concentration associated with non-ST5 infections at day 14
269 was driven by a single isolate - BMD1415. The TNF- α concentrations in lung homogenates
270 from mice infected with this isolate were significantly higher than for infections with any other
271 isolate of any lineage ($p < 0.001$). There was no statistically significant differences in TNF- α
272 concentrations at day 14 between lineages when this isolate was excluded from the analysis.
273 Similarly, the concentrations of these two cytokines in BMD1415-infected mice was significantly
274 higher than in mice infected with any other isolate ($p < 0.001$). However, the IL-12
275 concentrations declined in non-ST5-infected mice, including BMD1415, between day 7 and 14
276 (4 fold decrease, $p < 0.0001$) (Figure 5).

277
278 We measured the TNF- α :IL-10 ratio as a proxy for the relationship between a Th-1 and a Th-2
279 response²⁵. From day 7 to day 14 days post-infection, the TNF- α :IL-10 ratio decreased by a
280 factor of 0.78 in mice infected with ST5 isolates, while those infected with non-ST5 strains
281 exhibited an increase in the ratio of 1.25-fold. However, when BMD1415 (ST4) was excluded
282 from the analysis the TNF- α /IL-10 ratio in non-ST5 infected mice decreased by a factor of 0.67.
283 By day 14 we detected elevated concentrations of IL-17 and IFN- γ in non-ST5 infected mice (5-
284 fold and 17-fold increments, respectively (Table 4), but not in ST5 infected mice. Again, this

285 effect was largely associated with BMD1415, since the concentrations of IL-17 and IFN- γ
286 induced by this isolate at day 14 were significantly higher than for all others ($p < 0.001$).

287

288 *Histopathological examination*

289 Histological examination of infected lung tissue revealed evidence of inflammation,
290 hemorrhage, edema and necrosis in most cases. These changes were generally greater by day
291 14 in comparison to day 7. There were no clear differences in histological scores between ST,
292 other than with BMD1646 (ST5) which generated only mild inflammation with no evidence of
293 necrosis or hemorrhage (Figure S5). PAS staining revealed extensive perivascular infiltration of
294 leukocytes in mice tissue associated with both infecting genotypes (BMD1338-ST5 and
295 BMD1415-ST4, Figure 6). Extensive *in vivo* encapsulation of *C. neoformans* var. *grubii* in mouse
296 lung was visualized using Mucicarmine staining (Figure 7). However, it was unknown whether
297 the bigger capsule and cell size associated with ST5 organisms *in vitro*, as described earlier, was
298 also evident *in vivo* since we were unable to perform this measurement.

299

300 **Discussion**

301 Most cases of cryptococcal meningitis in HIV uninfected, apparently immunocompetent,
302 patients in Vietnam and East Asia are due to *C. neoformans* strains of multi-locus sequence type
303 5 (ST5)^{9,10,12,17,26–28}. This phenomenon could be explained either by ST5 strains being
304 intrinsically more pathogenic, or due to unidentified lineage-specific host immune defects or
305 exposures. It is unlikely that the high prevalence of ST5 infection observed in HIV-uninfected
306 patients is explained by a significantly greater prevalence of the lineage in the environment

307 since it causes only 35% of cases in HIV-infected patients within the same geographical area ⁹.
308 Furthermore, data from China suggest that ST5 strains are significantly less prevalent in the
309 environment, making up only 5% of isolates recovered in a recent study ²⁹. We investigated the
310 first hypothesis by comparing previously identified *in vitro* virulence-associated phenotypes,
311 along with murine *in vivo* virulence and immune responses, between lineages. All isolates were
312 derived from HIV infected or uninfected Vietnamese patients with cryptococcal meningitis. The
313 comparison by MLST defined lineage is appropriate because ST5 is a coherent and distinct
314 group, whole genome sequence data revealing that there are few intra-lineage genomic
315 variations between ST5 strains ¹⁷. More recent phylogenetic analysis using whole genome
316 sequencing of a larger collection of clinical isolates from Vietnam, including the eight strains
317 tested in the mouse model, has established that the MLST ST5 and ST4/ST6/306 groups are
318 genetically distinct lineages (VN1a-5 and VN1a-4, respectively) ¹⁵. It is unlikely that any
319 phenotypic variations among ST5 isolates are primarily attributable to *subtle* intra-lineage
320 genomic variations since phenotypic and genotypic diversity are not tightly coupled in *C.*
321 *neoformans* var. *grubii* ³⁰. Due to the fact that ST5 has been shown to be consistently associated
322 with the clinical phenotype of interest (infection in HIV-uninfected patients), and that strains
323 from HIV uninfected patients are dispersed throughout the VN1a-5 cluster, we believe the
324 ability to infect apparently immunocompetent hosts is common to all ST5 isolates. All
325 comparisons of ST versus non-ST5 in this study were thus essentially VN1a-5 versus VN1a-4.
326 We found that isolates from all STs were able to grow in *ex vivo* human CSF and at 37°C -
327 essential characteristics for establishing human CNS infection. While these qualities would be
328 needed for disease in both HIV infected and immunocompetent patients, it might have been

329 expected that ST5 strains would grow more rapidly in these conditions. The lack of ST-specific
330 differences in these phenotypes suggests that the ability to establish disease in HIV-
331 uninfected/immunocompetent patients is not driven by simple adaptations to these conditions.
332 Noticeably, ST5 cells were significantly larger than non-ST5 cells, had thicker capsules *in vitro*,
333 and had more within lineage variation in these characteristics. Capsule size and composition are
334 known to vary during infection and under specific stress conditions^{31,32}, influencing
335 macrophage phagocytosis and modulating host immune response³²⁻³⁵, and in human disease,
336 *ex vivo* capsule size has been associated with higher intracranial pressures, slower yeast
337 clearance and attenuated inflammation³⁴. While we did not formally measure yeast cell or
338 capsule size in our *in vivo* experiments, mucicarmine staining was suggestive that capsules were
339 indeed larger during mouse infection. It is possible that the ability of ST5 strains to cause
340 infections in immunocompetent patients is a function of increased responsiveness to capsule-
341 inducing conditions. Further investigation of genotype-specific characteristics of *in vitro* and *in*
342 *vivo* capsular polysaccharide production, composition, and morphology, may elucidate a
343 specific role in ST5-associated pathogenesis. Of note, cryptococcal virulence factors frequently
344 have additional metabolic functions; the increased cell and capsule size seen in ST5 isolates
345 may be a side effect of other processes involving capsular-biosynthesis genes (for example
346 carbon source sensing, sugar transport and spore formation)^{36,37}.

347 Our data indicate that phenotypic heterogeneity may be a hallmark characteristic of the ST5
348 lineage. Heterogeneity is a desirable trait for microbial populations under selection pressure
349 allowing the exploitation of, and survival, in novel niches³⁸. Chow *et al* (2008) has previously
350 reported that ST5 *C. neoformans* var. *grubii* possesses unique genomic features which may

351 drive niche adaptation³⁹. We speculate that the phenotypic heterogeneity associated with
352 strains from the ST5 lineage is a strategy that facilitates successful colonization of novel
353 environmental niches, including the exploitation of infrequent specific human immune deficits.
354 Morphological variation including cell size, capsule size and cell shape has also been associated
355 with different patient clinical symptoms, suggesting greater capacity for pathogenicity, immune
356 evasion and pathogenesis⁴⁰.

357 However, paradoxically, we found no evidence that ST5 isolates have greater virulence in the
358 mouse model. There are several possible explanations. First, virulence in mice is variable
359 depending on mouse breed and may not accurately reflect the immunological heterogeneity of
360 the human population⁴¹. Second, yeasts with different pathogenic potentials, associated with
361 their isolation from different sources (i.e. clinical versus environmental, immunocompromised
362 versus immunocompetent patients) may have the same or paradoxical pathogenic potential in
363 experimental animal models. An example is *Cryptococcus gattii* which is associated with
364 infection in immunocompetent patients and therefore is considered to be more fit in the
365 human host than *C. neoformans*. However, the hypervirulent *C. gattii* strain R265, responsible
366 for the on-going Vancouver outbreak, has similar virulence in both C57BL/6 and A/J mice to the
367 *C. neoformans* H99 strain, which was derived from a patient with Hodgkin's disease on
368 chemotherapy⁴². Third, the A/J mouse breed is not immunologically intact; it may be an
369 imperfect model of infection for immunocompetent hosts⁴³. Rather, A/J mice may be a better
370 model of disease in immunosuppressed patients, as they are highly susceptible to cryptococcal
371 disease, and the patterns of cytokine expression in mice with disseminated cryptococcosis are
372 similar to those seen in HIV-infected patients with CM⁴⁴. Consistent with this, we could not

373 detect clinical differences in disease course or outcome between HIV patients infected with ST5
374 versus other strains in Vietnam¹⁷. Models that better mimic infection in immunocompetent
375 hosts are needed.

376 We did identify lineage specific differences in immune response in the mouse model. Previous
377 research has suggested that a Th1 type immune response, defined by the TNF- α /IL-10 ratio, is
378 protective, and a Th2 response is associated with poor outcomes^{45,46}. We found no evidence of
379 genotype-specific differences in TNF- α /IL-10 ratios by lineage in the murine infection model.
380 Rather, we found higher initial (day 7) TNF- α concentrations in mice infected with ST5 isolates,
381 suggesting this genotype elicits a more intense initial inflammatory response. Previous studies
382 have suggested that capsule components, or cryptococcal cells themselves, have a dose-
383 dependent ability to stimulate TNF- α production by various immune effector cells^{47,48}. The
384 more robust initial inflammatory response we observed may have been due to the ST5 capsular
385 phenotype. Previously, it has been suggested that the ability of *C. gattii* to cause disease in
386 apparently immunocompetent patients is because it induces a less severe inflammatory
387 response compared with other cryptococcal species⁴². The robust initial inflammatory
388 responses seen in our murine infection experiments are not consistent with this being the
389 mechanism underlying the ability of ST5 *C. neoformans* var. *grubii* organisms to cause disease in
390 the immunocompetent.

391 *In vivo* controlled infection studies in mice, including ours, commonly employ the classic
392 definition of pathogenicity as the microbe's capability to cause disease in a susceptible host,
393 whereas virulence corresponds to the severity of the ensuing pathology⁴⁹. Using the same
394 infective dose for all strains we failed to demonstrate that ST5 strains had greater virulence.

395 The difference we observe in prevalence of different lineages in immunocompetent and
396 immunosuppressed humans may actually represent specific differences in pathogenicity - the
397 ability of the organisms to colonize the host and establish infection. We could not assess this
398 with our experimental system.

399 In summary, our cohort of ST5 *Cryptococcus* isolates displayed two notable phenotypes. First,
400 despite their well-documented ability to cause disease in HIV uninfected humans, they
401 appeared to be less virulent in a murine model than the other sequence types, as demonstrated
402 by reduced fungal burdens in tissue and prolonged mouse survival. Second, ST5 strains had
403 larger capsules and cell sizes than the other genotypes, and greater variability in this phenotype
404 throughout the lineage. These data lead us to the following conclusions. First, clinical isolates,
405 which have by their nature already undergone selection within the human host, can possess
406 wide variability in the expression of virulence phenotypes within a single lineage. Secondly, the
407 use of host risk factors and immune phenotypes to derive an understanding of the factors that
408 drive the pathogenicity of *Cryptococcus neoformans* may be more complex than anticipated.

409 Associations may be difficult to make due to the relevance of the particular *in vitro* phenotypes,
410 the animal models used, within strain heterogeneity, and population substructure. Moreover,
411 there may be heterogeneity in the immune response of apparently immunocompetent patients
412 which selects particular sub-cohorts of isolates of the same lineage. Laboratory phenotyping of
413 larger numbers of clinical isolates is needed to define the lineage-specific differences that
414 determine different human disease phenotypes.

415 Finally, it is possible that the categorization of strains into specific clades with limited genetic
416 information such as MLST may lack precision to understand the relative fitness of specific

417 strains in the human host. It is likely that whole genome sequencing will provide better
418 mapping of the relationships between strains and virulence.

419 In conclusion, in this study, we demonstrated genotype-specific differences in *in vitro* and *in*
420 *vivo* virulence phenotypes between *C. neoformans* var. *grubii* strains isolated from host with
421 different immune status. However, there was also significant variation among strains isolated
422 from apparently immunocompetent patients in specific *in vitro* and *in vivo* phenotypes tested.
423 This higher rate of phenotypic variation may represent an evolutionary strategy for *C.*
424 *neoformans* var. *grubii* to take advantage of novel niches and contribute to their ability to infect
425 apparently immunocompetent hosts, despite generally being less virulent in a mammalian
426 animal model. Furthering the understanding of the pathogenesis of cryptococcal meningitis will
427 require investigation of large numbers of strains with associated robust clinical information,
428 and the development of high throughput laboratory phenotypic studies that have clinical
429 relevance in humans.

430 **Acknowledgements**

431 This work was supported by a Wellcome Trust Intermediate Fellowship awarded to JND
432 (WT097147MA), and a Henry Dale Fellowship jointly funded by the Wellcome Trust and the
433 Royal Society (100087/Z/12/Z) awarded to SGB. Multiplex cytokine profiling was performed in
434 the Immunology Unit of the Duke Regional Biocontainment Laboratory, which received partial
435 support for construction from the US National Institutes of Health, National Institute of Allergy
436 and Infectious Diseases (UC6-AI058607). The study was approved by the scientific committee of
437 the Hospital for Tropical Diseases, Ho Chi Minh City, Vietnam.

438

439 **Conflicts of Interest**

440 None

441

442 **References**

- 443 1. Fang W, Chen M, Liu J, et al. Cryptococcal meningitis in systemic lupus erythematosus
444 patients: pooled analysis and systematic review. *Emerg Microbes Infect.* 2016;5(9):e95.
445 doi:10.1038/emi.2016.93
- 446 2. Schmalzle SA, Buchwald UK, Gilliam BL, Riedel DJ. *Cryptococcus neoformans* infection in
447 malignancy. *Mycoses.* 2016;59(9):542-552. doi:10.1111/myc.12496
- 448 3. Williamson PR, Jarvis JN, Panackal AA, et al. Cryptococcal meningitis: epidemiology,
449 immunology, diagnosis and therapy. *Nat Rev Neurol.* 2016;13(1):13-24.
450 doi:10.1038/nrneurol.2016.167
- 451 4. Rajasingham R, Smith RM, Park BJ, et al. Global burden of disease of HIV-associated
452 cryptococcal meningitis: an updated analysis. *Lancet Infect Dis.* 2017;17(8):873-881.
453 doi:10.1016/S1473-3099(17)30243-8
- 454 5. Kwon-Chung KJ, Fraser JA, Doering TL, et al. *Cryptococcus neoformans* and *Cryptococcus*
455 *gattii*, the etiologic agents of cryptococcosis. *Cold Spring Harb Perspect Med.*
456 2014;4(7):a019760. doi:10.1101/cshperspect.a019760
- 457 6. Pappas PG. Cryptococcal infections in non-HIV-infected patients. *Trans Am Clin Climatol*
458 *Assoc.* 2013;124:61-79.
- 459 7. Shih CC, Chen YC, Chang SC, Luh KT, Hsieh WC. Cryptococcal meningitis in non-HIV-
460 infected patients. *QJM.* 2000;93(4):245-251. doi:10.1093/qjmed/93.4.245

- 461 8. Chau TT, Mai NH, Phu NH, et al. A prospective descriptive study of cryptococcal
462 meningitis in HIV uninfected patients in Vietnam - high prevalence of *Cryptococcus*
463 *neoformans* var. *grubii* in the absence of underlying disease. *BMC Infect Dis.*
464 2010;10(1):199. doi:10.1186/1471-2334-10-199
- 465 9. Day JN, Hoang TN, Duong A V, et al. Most cases of cryptococcal meningitis in HIV-
466 uninfected patients in Vietnam are due to a distinct amplified fragment length
467 polymorphism-defined cluster of *Cryptococcus neoformans* var. *grubii* VN1. *J Clin*
468 *Microbiol.* 2011;49(2):658-664. doi:10.1128/JCM.01985-10
- 469 10. Chen J, Varma A, Diaz M. *Cryptococcus neoformans* strains and infection in apparently
470 immunocompetent patients, China. *Emerg Infect Dis.* 2008;14(5).
- 471 11. Li Z, Liu Y, Cao H, Huang S, Long M. Epidemiology and clinical characteristics of
472 cryptococcal meningitis in china (1981-2013): A review of the literature. *Med Mycol*
473 *Open Access.* 2017;3(1):1-6. doi:10.4172/2471-8521.100022
- 474 12. Fan X, Xiao M, Chen S-L, et al. Predominance of *Cryptococcus neoformans* var. *grubii*
475 multilocus sequence type 5 and emergence of isolates with non-wild-type minimum
476 inhibitory concentrations to fluconazole: a multi-centre study in China. *Clin Microbiol*
477 *Infect.* 2016;22(10):887.e1-887.e9. doi:10.1016/j.cmi.2016.07.008
- 478 13. Dou H-T, Xu Y-C, Wang H-Z, Li T-S. Molecular epidemiology of *Cryptococcus neoformans*
479 and *Cryptococcus gattii* in China between 2007 and 2013 using multilocus sequence
480 typing and the DiversiLab system. *Eur J Clin Microbiol Infect Dis.* 2015;34(4):753-762.
481 doi:10.1007/s10096-014-2289-2
- 482 14. Choi YH, Ngamskulrungraj P, Varma A, et al. Prevalence of the VN1c genotype of

- 483 *Cryptococcus neoformans* in non-HIV-associated cryptococcosis in the Republic of Korea.
484 *FEMS Yeast Res.* 2010;10(6):769-778. doi:10.1111/j.1567-1364.2010.00648.x
- 485 15. Ashton PM, Thanh LT, Trieu PH, et al. Three phylogenetic groups have driven the recent
486 population expansion of *Cryptococcus neoformans*. *Nat Commun.* 2019;10(1):1-10.
487 doi:10.1038/s41467-019-10092-5
- 488 16. Day JN, Chau TTH, Wolbers M, et al. Combination antifungal therapy for cryptococcal
489 meningitis. *N Engl J Med.* 2013;368(14):1291-1302. doi:10.1056/NEJMoa1110404
- 490 17. Day JN, Qihui S, Thanh LT, et al. Comparative genomics of *Cryptococcus neoformans* var.
491 *grubii* associated with meningitis in HIV infected and uninfected patients in Vietnam.
492 *PLoS Negl Trop Dis.* 2017;11(6):e0005628. doi:10.1371/journal.pntd.0005628
- 493 18. Lee A, Toffaletti DL, Tenor J, et al. Survival defects of *Cryptococcus neoformans* mutants
494 exposed to human cerebrospinal fluid result in attenuated virulence in an experimental
495 model of meningitis. *Infect Immun.* 2010;78(10):4213-4225. doi:10.1128/IAI.00551-10
- 496 19. Idnurm A, Walton FJ, Floyd A, Reedy JL, Heitman J. Identification of ENA1 as a virulence
497 gene of the human pathogenic fungus *Cryptococcus neoformans* through signature-
498 tagged insertional mutagenesis. *Eukaryot Cell.* 2009;8(3):315-326. doi:10.1128/EC.00375-
499 08
- 500 20. Salas SD, Bennett JE, Kwon-Chung KJ, Perfect JR, Williamson PR. Effect of the laccase
501 gene CNLAC1, on virulence of *Cryptococcus neoformans*. *J Exp Med.*
502 1996;184(August):377-386. doi:10.1084/jem.184.2.377
- 503 21. Eisenman HC, Mues M, Weber SE, et al. *Cryptococcus neoformans* laccase catalyses
504 melanin synthesis from both D- and L-DOPA. *Microbiology.* 2007;153(12):3954-3962.

- 505 doi:10.1099/mic.0.2007/011049-0
- 506 22. Chen SC, Muller M, Zhou JZ, Wright LC, Sorrell TC. Phospholipase activity in *Cryptococcus*
507 *neoformans*: a new virulence factor? *J Infect Dis.* 1997;175(2):414-420.
508 doi:10.1093/infdis/175.2.414
- 509 23. Zaragoza O, Casadevall A. Experimental modulation of capsule size in *Cryptococcus*
510 *neoformans*. *Biol Proced Online.* 2004;6(1):10-15. doi:10.1251/bpo68
- 511 24. Hu G, Cheng P-Y, Sham A, Perfect JR, Kronstad JW. Metabolic adaptation in *Cryptococcus*
512 *neoformans* during early murine pulmonary infection. *Mol Microbiol.* 2008;69(6):1456-
513 1475. doi:10.1111/j.1365-2958.2008.06374.x
- 514 25. Levitz SM, Tabuni A, Nong SH, Golenbock DT. Effects of interleukin-10 on human
515 peripheral blood mononuclear cell responses to *Cryptococcus neoformans*, *Candida*
516 *albicans*, and lipopolysaccharide. *Infect Immun.* 1996;64(3):945-951.
- 517 26. Fang W, Fa Z, Liao W. Epidemiology of *Cryptococcus* and cryptococcosis in China. *Fungal*
518 *Genet Biol.* November 2014. doi:10.1016/j.fgb.2014.10.017
- 519 27. Khayhan K, Hagen F, Pan W, et al. Geographically structured populations of *Cryptococcus*
520 *neoformans* variety *grubii* in Asia correlate with HIV status and show a clonal population
521 structure. Zaragoza O, ed. *PLoS One.* 2013;8(9):e72222.
522 doi:10.1371/journal.pone.0072222
- 523 28. Chen M, Xu Y, Hong N, et al. Epidemiology of fungal infections in China. *Front Med.*
524 2018;12(1):58-75. doi:10.1007/s11684-017-0601-0
- 525 29. Dou H, Wang H, Xie S, Chen X, Xu Z, Xu Y. Molecular characterization of *Cryptococcus*
526 *neoformans* isolated from the environment in Beijing, China. *Med Mycol.* 2017;38:1-11.

- 527 doi:10.1093/mmy/myx026
- 528 30. Beale MA, Sabiiti W, Robertson EJ, et al. Genotypic diversity is associated with clinical
529 outcome and phenotype in cryptococcal meningitis across Southern Africa. Vinetz JM,
530 ed. *PLoS Negl Trop Dis*. 2015;9(6):e0003847. doi:10.1371/journal.pntd.0003847
- 531 31. Bojarczuk A, Miller KA, Hotham R, et al. *Cryptococcus neoformans* intracellular
532 proliferation and capsule size determines early macrophage control of infection. *Sci Rep*.
533 2016;6(October 2015):21489. doi:10.1038/srep21489
- 534 32. Zaragoza O, Chrisman CJ, Castelli MV, et al. Capsule enlargement in *Cryptococcus*
535 *neoformans* confers resistance to oxidative stress suggesting a mechanism for
536 intracellular survival. *Cell Microbiol*. 2008;10(10):2043-2057. doi:10.1111/j.1462-
537 5822.2008.01186.x
- 538 33. García-Rodas R, Casadevall A, Rodríguez-Tudela JL, Cuenca-Estrella M, Zaragoza O.
539 *Cryptococcus neoformans* capsular enlargement and cellular gigantism during *Galleria*
540 *mellonella* infection. *PLoS One*. 2011;6(9):e24485. doi:10.1371/journal.pone.0024485
- 541 34. Robertson EJ, Najjuka G, Rolfes M a, et al. *Cryptococcus neoformans* ex vivo capsule size
542 is associated with intracranial pressure and host immune response in HIV-associated
543 cryptococcal meningitis. *J Infect Dis*. 2014;209(1):74-82. doi:10.1093/infdis/jit435
- 544 35. Vecchiarelli A, Pericolini E, Gabrielli E, et al. *Cryptococcus neoformans* galactoxylomannan
545 is a potent negative immunomodulator, inspiring new approaches in anti-inflammatory
546 immunotherapy. *Immunotherapy*. 2011;3:997-1005. doi:10.2217/imt.11.86
- 547 36. Kronstad J, Saikia S, Nielson ED, et al. Adaptation of *Cryptococcus neoformans* to
548 mammalian hosts: integrated regulation of metabolism and virulence. *Eukaryot Cell*.

- 549 2012;11(2):109-118. doi:10.1128/EC.05273-11
- 550 37. Botts MR, Giles SS, Gates MA, Kozel TR, Hull CM. Isolation and characterization of
551 *Cryptococcus neoformans* spores reveal a critical role for capsule biosynthesis genes in
552 spore biogenesis. *Eukaryot Cell*. 2009;8(4):595-605. doi:10.1128/EC.00352-08
- 553 38. Bódi Z, Farkas Z, Nevozhay D, et al. Phenotypic heterogeneity promotes adaptive
554 evolution. *PLoS Biol*. 2017;15(5):e2000644. doi:10.1371/journal.pbio.2000644
- 555 39. Chow EWL, Morrow CA, Djordjevic JT, Wood IA, Fraser JA. Microevolution of
556 *Cryptococcus neoformans* driven by massive tandem gene amplification. *Mol Biol Evol*.
557 2012;29(8):1987-2000. doi:10.1093/molbev/mss066
- 558 40. Fernandes KE, Brockway A, Haverkamp M, et al. Phenotypic variability correlates with
559 clinical outcome in *Cryptococcus* isolates obtained from Botswanan HIV/AIDS Patients.
560 *MBio*. 2018;9(5):e02016-18. doi:10.1128/mBio.02016-18
- 561 41. Zaragoza O, Alvarez M, Telzak A, Rivera J, Casadevall A. The relative susceptibility of
562 mouse strains to pulmonary *Cryptococcus neoformans* infection is associated with
563 pleiotropic differences in the immune response. *Infect Immun*. 2007;75(6):2729-2739.
564 doi:10.1128/IAI.00094-07
- 565 42. Cheng P-Y, Sham A, Kronstad JW. *Cryptococcus gattii* isolates from the British Columbia
566 cryptococcosis outbreak induce less protective inflammation in a murine model of
567 infection than *Cryptococcus neoformans*. *Infect Immun*. 2009;77(10):4284-4294.
568 doi:10.1128/IAI.00628-09
- 569 43. Sellers RS, Clifford CB, Treuting PM, Brayton C. Immunological variation between inbred
570 laboratory mouse strains: points to consider in phenotyping genetically immunomodified

- 571 mice. *Vet Pathol.* 2012;49(1):32-43. doi:10.1177/0300985811429314
- 572 44. Lortholary O, Improvisi L, Rayhane N, et al. Cytokine profiles of AIDS patients are similar
573 to those of mice with disseminated *Cryptococcus neoformans* infection. *Infect Immun.*
574 1999;67(12):6314-6320.
- 575 45. Jain A V, Zhang Y, Fields WB, et al. Th2 but not Th1 immune bias results in altered lung
576 functions in a murine model of pulmonary *Cryptococcus neoformans* infection. *Infect*
577 *Immun.* 2009;77(12):5389-5399. doi:10.1128/IAI.00809-09
- 578 46. Koguchi Y, Kawakami K. Cryptococcal infection and Th1-Th2 cytokine balance. *Int Rev*
579 *Immunol.* 2002;21(4-5):423-438. doi:10.1080/08830180190048109
- 580 47. Chaka W, Verheul AF, Vaishnav V V, et al. *Cryptococcus neoformans* and cryptococcal
581 glucuronoxylomannan, galactoxylomannan, and mannoprotein induce different levels of
582 tumor necrosis factor alpha in human peripheral blood mononuclear cells. *Infect Immun.*
583 1997;65(1):272-278.
- 584 48. Levitz SM, Tabuni A, Kornfeld H, Reardon CC, Golenbock DT. Production of tumor
585 necrosis factor alpha in human leukocytes stimulated by *Cryptococcus neoformans*. *Infect*
586 *Immun.* 1994;62(5):1975-1981.
- 587 49. García-Rivera J, Casadevall A. Melanization of *Cryptococcus neoformans* reduces its
588 susceptibility to the antimicrobial effects of silver nitrate. *Med Mycol.* 2001;39:353-357.
589 doi:10.1080/mmy.39.4.353.357
- 590
- 591
- 592

593

594

595

596 **FIGURE LEGENDS**

597 **Figure 1. *In vitro* induced capsule thickness and cell diameter of individual *Cryptococcus***

598 ***neoformans* strains from Vietnam:** Cells were grown on DMEM medium/5% CO₂ and visually

599 assessed by India ink staining. Images were taken for single cells measurement using ImageJ

600 software. Capsule thickness is obtained by subtracting cell body diameter from total cell

601 diameter. AFLP-VNI-γ/MLST-ST5 strains expressed higher degree of variation in both capsule

602 size and cell diameter *in vitro*, which remains significant even when the outlier BMD1646 was

603 removed from the analysis ($p < 0.0001$ for both capsule and cell size, Fligner-Killeen test).

604 Scattered plot represents single cells from an individual strain. Data for individual strains are

605 presented as mean with error bars denoting standard deviation. Strains selected for experiment

606 in mice were indicated by asterisks.

607

608 **Figure 2. Kaplan-Meier survival curves for mice infected with either ST5 (n = 5) or non-ST5 (n=**

609 **3) *Cryptococcus neoformans* strains.** 10 A/J mice were infected per strain (five ST5 strains and

610 three non-ST5 strains). Mice were monitored daily until the point of more than 15% weight loss

611 or visible suffering and were then sacrificed by CO₂ inhalation. Mice infected with ST5 strains

612 had statistically significantly longer survival times than those infected with non-ST5 strains

613 ($P < 0.0001$, Mantel-Cox log rank test) (Panel A). Two ST5 strains, BK147 and BMD1646, were

614 attenuated, suggesting high degree of heterogeneity within the ST5 cluster. Mice infected with

615 BK147 and BMD1646 survived for as long as 42 days post-infection, at which point the
616 experiment was terminated and all infected mice sacrificed (Panel B).

617

618 **Figure 3. Fungal burden in mouse lung and brain tissue at days 7, 14 and the point of**
619 **impending death (mortality experiment) according to infecting genotype.** *In vivo* virulence
620 (tissue fungal burden and mortality) was assessed in three independent mouse infection
621 experiments. In the first two experiments, five A/J mice were infected with each of the eight
622 test *C. neoformans* isolate (five ST5 isolates and 3 non-ST5 isolates, total N=40 mice in each
623 experiment). All mice were sacrificed at day 7 post-infection in the first experiment and at day
624 14 post-infection in the second experiment to assess *in vivo* fungal burden in mouse lung and
625 brain. Fungal burden in the lung and brain at either day 7 or day 14 for each isolate is presented
626 in panel A. In the last experiment, ten A/J mice were infected with each of the 8 test *C.*
627 *neoformans* isolate (five ST5 isolates and 3 non-ST5 isolates, N=80 mice in total) and monitored
628 daily until the point when 15% of body weight loss, a sign of distress and impending death, was
629 evident. Fungal burden in lung and brain at point of death was again assessed as before. Here,
630 for each strain, five mice were randomly selected from the ten test mice for fungal burden
631 investigation. The pooled fungal burden in non-ST5 infections was higher than in ST5 infections
632 in both lung tissue at all time points, and in brain tissue at the point of sacrifice (Panel B) (For P
633 values see text). Boxplots (Tukey's method) describe the median and interquartile range, the
634 whiskers demarcate the largest or smallest values that were not outliers (black dots); outliers
635 are defined as more than 1.5 times the interquartile range from the nearest quartile.

636

637 **Figure 4. Genotype-specific cytokine concentrations from lung homogenate of A/J mice at 7**
638 **and 14 days post infection with 5×10^4 *C. neoformans* cells/mouse.** Five mice were infected
639 with each strain from each genotype at each time points. ST5 strains induced significantly
640 higher levels of TNF- α at day 7, suggesting an earlier and more profound initial inflammatory
641 response in infected mice. By day 14 mice infected with non-ST5 strains have higher levels
642 proinflammatory cytokines, probably a result of ST5 yeasts being cleared more rapidly from
643 infected mice. The horizontal line within the box indicates the median; boundaries of the box
644 indicate the 25th and 75th percentile and the whiskers indicate the highest and lowest values of
645 the results; outliers are denoted as black dots (Tukey's method). Data are standardized as
646 picograms of cytokine per gram lung tissue. Asterisks indicate statistically significant differences
647 (Mann-Whitney test).

648

649 **Figure 5. Genotype-specific changes in cytokine concentrations from lung homogenate of A/J**
650 **mice infected with *C. neoformans* between day 7 and day 14 post-infection.** Box and whisker
651 plots (Tukey's method) compare levels of each cytokine between day 7 and day 14 for each
652 genotype. Data are standardized as picograms of cytokine per gram lung tissue. Asterisks
653 indicate statistically significant differences (Mann-Whitney test).

654

655 **Figure 6. Periodic Acid Schiff (PAS) staining of pulmonary tissue from mice infected with**
656 **BMD1338 and BMD1415 on days 7 and 14.** The two strains represent ST5 and non-ST5,
657 respectively. A/J mice were inoculated intranasally with 5×10^4 yeast cells. Lung specimens were

658 harvested at days 7 and 14 for histopathological examination. Photomicrographs were obtained
659 at 200X magnification; the scale bar represents 215 μm). (A-B): lung sections from mice infected
660 with BMD1338 (VNI- γ /ST5) at day 7 and day 14, respectively. (C-D): lung sections from mice
661 infected with BMD1415 (VNI- δ /ST4) at day 7 and day 14, respectively. Perivascular infiltration
662 (red arrows) and necrosis are more marked by day 14 for both strains. Encapsulated yeasts
663 (yellow arrows), notable for the larger cell size and capsule thickness of BMD 1338 compared
664 with BMD1415.

665

666 **Figure 7. Mucicarmine staining of capsular material in paraffin-embedded mice pulmonary**
667 **tissue.**

668 Uninflated lung specimens were harvested from mice as described in the methods.

669 Mucicarmine staining was performed to visualize the cryptococcal capsule. Photomicrographs
670 were captured at 400X magnification with scale bar indicating 55 μm . Capsular polysaccharide is
671 stained pink (indicated by blue arrows), demonstrating diffuse localization consistent with
672 extensive capsule production by yeasts in the alveolar space.

673 **FIGURE S1. Phenotyping of *C. neoformans* var. *grubii* isolates from Vietnam (ST5: n=15 and**
674 **non-ST5: n=15).** Data were obtained from 30 isolates (15 ST5 and 15 non-ST5) in 3 different
675 experiment batches, with 3 technical replicates of each isolate per batch. Data are expressed as
676 the ratio between measurements of the test isolates and that of H99. Boxplots (Tukey's
677 method) describe the median and interquartile range (panel A-C). For assessment of urease
678 activity (panel D), we used the time to complete color change of the agar plate as an indirect
679 measure of extracellular urease activity since all *C. neoformans* var. *grubii* isolates in our

680 collection were positive for urease activity. Each isolate were tested in triplicate and monitored
681 in real time by live-imaging. No significant difference in any virulence-associated phenotype
682 were observed between the two MLST groups.

683 **FIGURE S2. Growth at different temperature of 8 *C. neoformans* (five ST5 and three non-ST5)**
684 **isolates from Vietnamese patients used in the murine infection experiments.** All strains
685 expressed similar growth at 30°C. Two ST5 isolates (BMD1646 and BK147) displayed diminished
686 growth at 37°C compared to other test isolates.

687 **FIGURE S3. *Ex vivo* growth in human cerebrospinal fluid (CSF) of 8 clinical *C. neoformans***
688 **isolates from Vietnamese patients that were tested for virulence in mice, representing both**
689 **ST5 (n = 5) and non-ST5 (n = 3) genotypes.** The same inoculum of yeasts were inoculated in
690 pooled human CSF and incubated at 37°C. The inoculated CSF was serially diluted and plated on
691 YPD agar at day 1 and day 3 post-inoculation. The wild-type H99 strain and the H99-derived
692 mutant *Δena1*, lacking a cation ATPase transporter which results in decreased viability in
693 human CSF and within macrophages, were included as controls. An apparent difference in
694 growth between ST5 and non-ST5 isolates could be observed at day 3.

695 **FIGURE S4. Melanin production on L-DOPA medium of eight clinical *C. neoformans* isolates**
696 **from Vietnamese patients representing both ST5 (n =5) and non-ST5 (n = 3) genotypes that**
697 **were tested for virulence in mice.** For each isolates, 10µl of 10⁶ cell suspension was inoculated
698 on L-DOPA agar and incubated in the dark at 30°C and 37°C. No clear genotype-specific patterns
699 of melanization were observed at either 30°C or 37°C. The five ST5 strains displayed marked

700 variation in the degree of pigment production, from mildly melanized (BK147) to highly
701 melanized (BK44 and BMD1646).

702 **FIGURE S5: Histopathological scores across 4 categories of tissue damage (Inflammation,**
703 **necrosis, hemorrhage and edema).** Thin sections of paraffin-embedded lung specimens from
704 infected mice were stained using the Periodic Acid Schiff (PAS) method. Specimens were
705 assessed by an independent pathologist who was blind to infecting isolate and in randomized
706 order. Scores ranged from 0 (no changes) to 10 (severe changes), corresponding to the severity
707 of pathology in in each category as per the Duke Veterinary Diagnostic Laboratory protocol
708 (Division of Laboratory Animal Resources).

709

710

711

712

713

714

715

716

717

718

719

720

721 **TABLES**

722 **TABLE 1** *Cryptococcus neoformans* isolate clinical source and typing (n=30).

Isolate data			Patient data		
Order	Strain name	WGS	MLST	Underlying Disease	Sex
		cluster	sequence type		
1	BK14	VNIa-4	4	HIV	M
2	BK163	VNIa-4	4	HIV	M
4	BK225	VNIa-4	4	HIV	M
6	BK48	VNIa-4	4	HIV	M
7	BK59	VNIa-4	4	HIV	F
8	BK69	VNIa-4	4	HIV	M
9	BK74	VNIa-4	4	HIV	M
10	BK80*	VNIa-4	4	HIV	M
11	BK87	VNIa-4	4	HIV	M
12	BK88	VNIa-4	4	HIV	M
13	BK89	VNIa-4	4	HIV	M
15	BMD1415*	VNIa-4	4	Lupus	M
3	BK218	VNIa-4	6	HIV	M
5	BK234	VNIa-4	6	HIV	F
14	BMD1367*	VNIa-4	306	Gastric cancer	F

16	BK147*	VNIa-5	5	HIV	M
17	BK44*	VNIa-5	5	HIV	M
18	BMD101	VNIa-5	5	None known	M
19	BMD1228	VNIa-5	5	None known	F
20	BMD1291	VNIa-5	5	None known	F
21	BMD1338*	VNIa-5	5	None known	M
22	BMD1353	VNIa-5	5	None known	M
23	BMD1452	VNIa-5	5	None known	F
24	BMD1646*	VNIa-5	5	None known	M
25	BMD1716	VNIa-5	5	None known	F
26	BMD367	VNIa-5	5	None known	M
27	BMD673	VNIa-5	5	None known	F
28	BMD700*	VNIa-5	5	None known	M
29	BMD854	VNIa-5	5	None known	F
30	BMD899	VNIa-5	5	None known	F

WGS = whole genome sequencing

MLST = multi locus sequence typing

M = Male, F = Female

** indicates isolates selected for mouse experiment*

723

724

725 **TABLE 2** Variability in *in vitro* capsule thickness and cell diameter of *Cryptococcus neoformans*
726 strains by Sequence Type (ST)

727

Variable	MLST Group	
	ST5	Non-ST5
Capsule Thickness (μm)		
Mean*	2.64	2.01
95% CI	2.49 - 2.79	1.94 - 2.07
Range	0.01 - 9.56	0.02 - 6.16
Coefficient of Variation [§]		
(%)	0.63	0.37
Cell diameter (μm)		
Mean*	11.38	9.69
95% CI of Mean	10.96 - 11.79	9.52 - 9.87
Range	4.74 - 27.22	5.25 - 19.89
Coefficient of Variation [§]		
(%)	0.41	0.20

728 * $P < 0.0001$, *t*-test with Welch's correction.

729 [§] $P < 0.0001$, *Fligner-Killeen test of homogeneity of variance*.

730

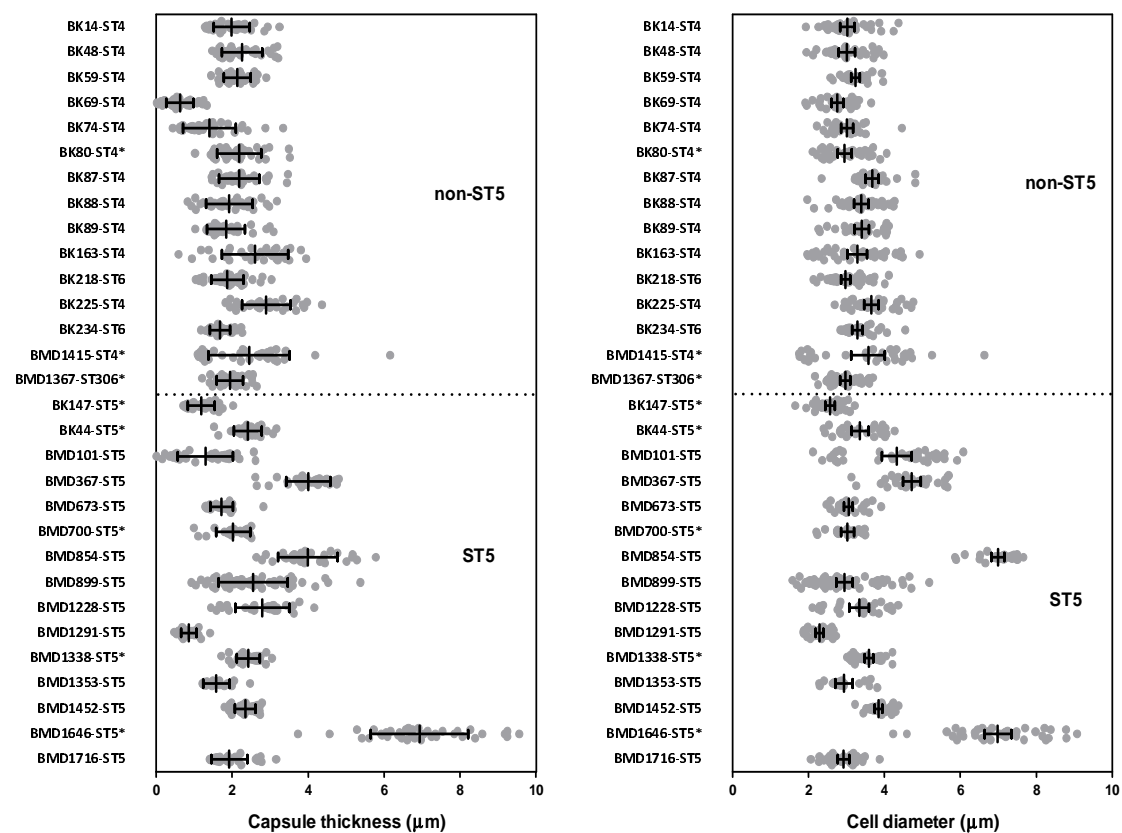
731

732 **TABLE 3** Tissue fungal burden in lung and brains of mice at days 7, 14 and at time of death by
 733 infecting MLST Sequence Type (ST)

Fungal burden
 (Mean log₁₀ colony forming units per gram of
 tissue)
 [95%CI]

Tissue	ST5	Non-ST5	P Value
Lung (Day 7)	4.96 [3.86 - 6.05]	7.07 [6.85 - 7.29]*	<0.001
Brain (Day 7)	0.81 [0.38 - 1.24]	1.59 [0.87 - 2.30]	0.054
Lung (Day 14)	5.48 [4.34 - 6.62]	8.00 [7.77 - 8.23]*	<0.0001
Brain (Day 14)	1.56 [0.81 - 2.31]	1.91 [1.12 - 2.69]	0.36
Lung (Death)	3.81 [3.05 - 4.57]	6.53 [6.30 - 6.76]*	<0.0001
Brain (Death)	2.90 [2.23 - 3.56]	4.29 [3.90 - 4.68]*	0.01

*Mann-Whitney test.



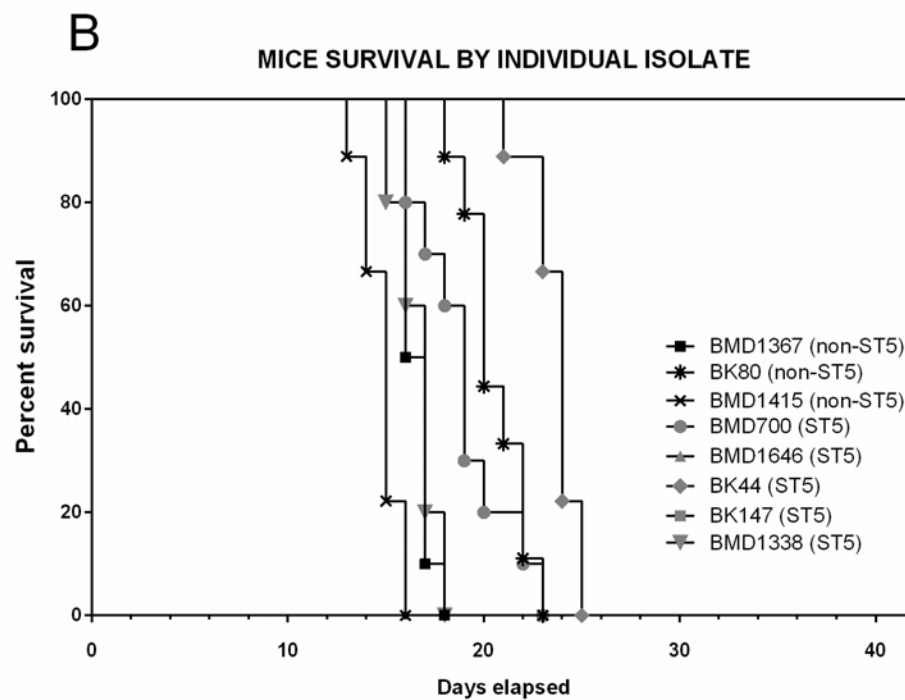
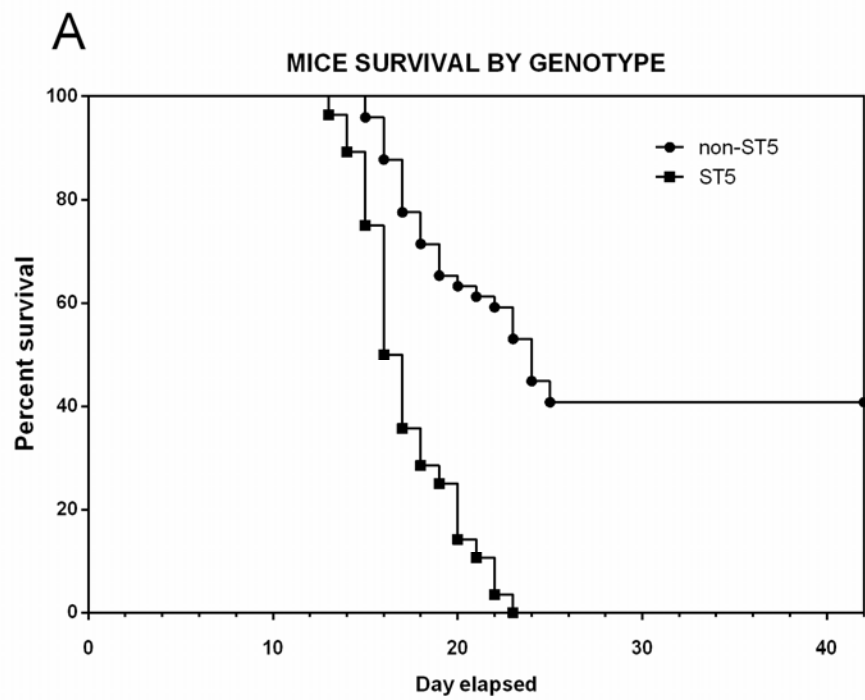
734

735 **Figure 2. *In vitro* induced capsule thickness and cell diameter of individual *Cryptococcus neoformans* strains from Vietnam:** Cells were grown

736 on DMEM medium/5% CO₂ and visually assessed by India ink staining. Images were taken for single cells measurement using ImageJ software.

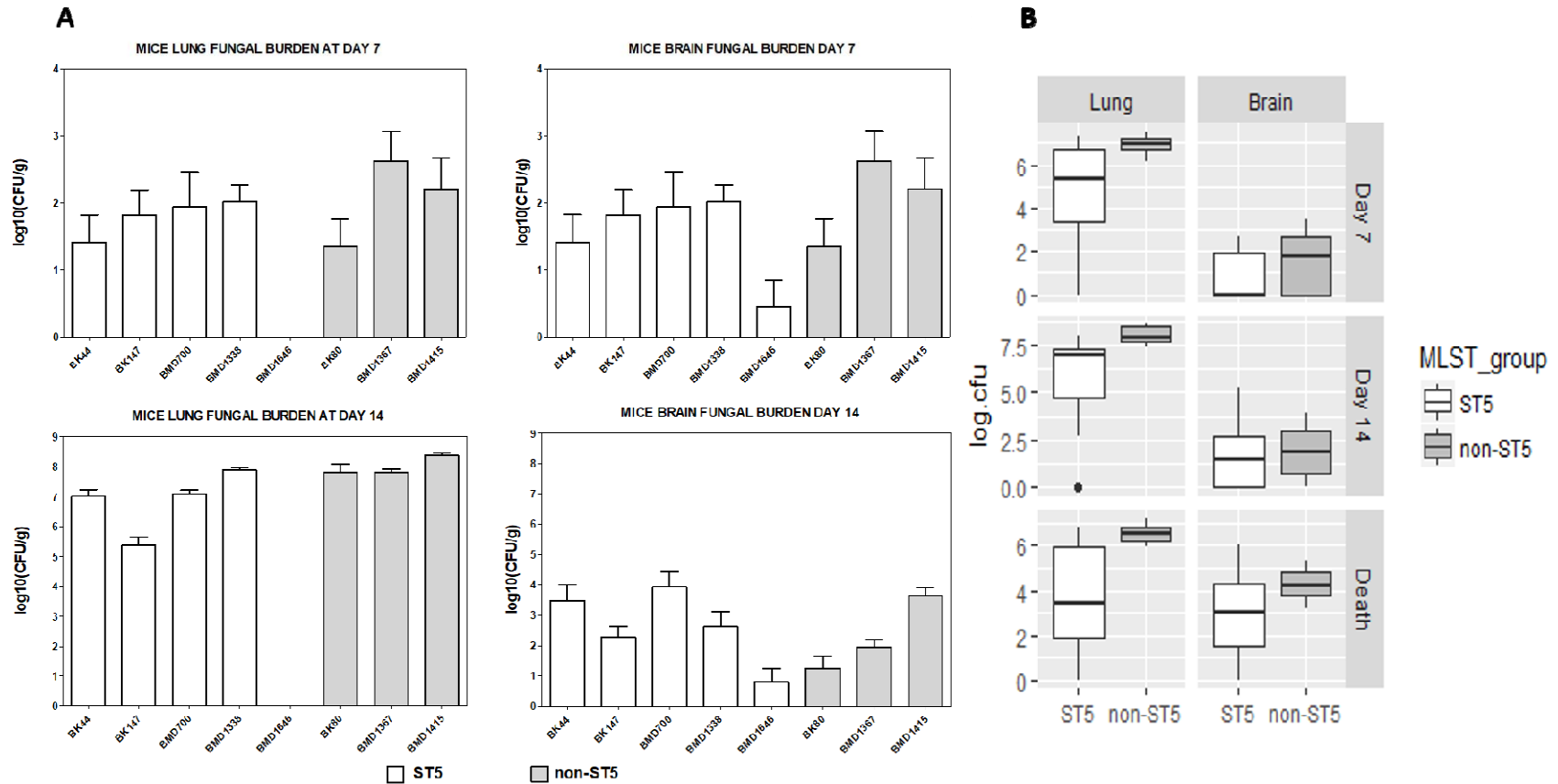
737 Capsule thickness is obtained by subtracting cell body diameter from total cell diameter. AFLP-VNI-γ/MLST-ST5 strains expressed higher degree
738 of variation in both capsule size and cell diameter *in vitro*, which remains significant even when the outlier BMD1646 was removed from the
739 analysis ($p < 0.0001$ for both capsule and cell size, Fligner-Killeen test). Scattered plot represents single cells from an individual strain. Data for
740 individual strains are presented as mean with error bars denoting standard deviation. Strains selected for experiment in mice were indicated by
741 asterisks.

742



744 **Figure 2. Kaplan-Meier survival curves for mice infected with either ST5 (n = 5) or non-ST5 (n= 3) *Cryptococcus neoformans* strains.** 10
745 A/J mice were infected per strain (five ST5 strains and three non-ST5 strains). Mice were monitored daily until the point of more than 15%
746 weight loss or visible suffering and were then sacrificed by CO₂ inhalation. Mice infected with ST5 strains had statistically significantly longer
747 survival times than those infected with non-ST5 strains (P<0.0001, Mantel-Cox log rank test) (Panel A). Two ST5 strains, BK147 and
748 BMD1646, were attenuated, suggesting high degree of heterogeneity within the ST5 cluster. Mice infected with BK147 and BMD1646 survived
749 for as long as 42 days post-infection, at which point the experiment was terminated and all infected mice sacrificed (Panel B).
750

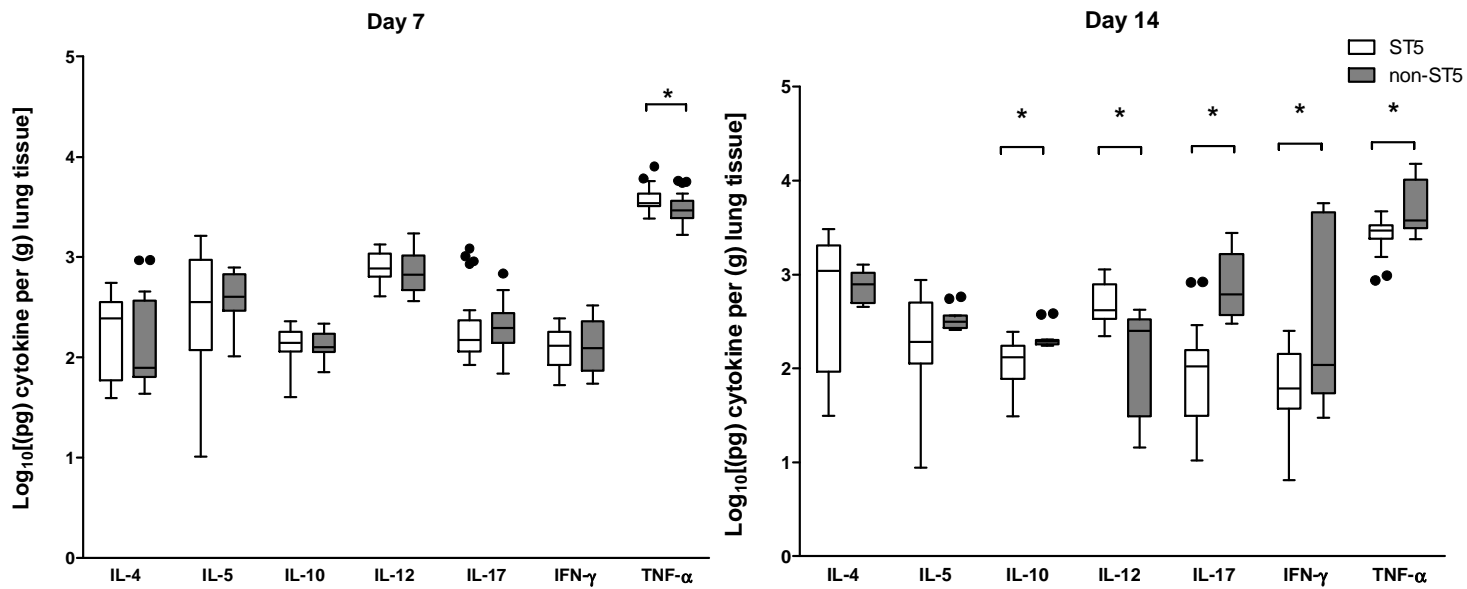
751



752

753 **Figure 3. Fungal burden in mouse lung and brain tissue at days 7, 14 and the point of impending death (mortality experiment) according to**
 754 **infecting genotype.** *In vivo* virulence (tissue fungal burden and mortality) was assessed in three independent mouse infection experiments. In
 755 the first two experiments, five A/J mice were infected with each of the eight test *C. neoformans* isolates (five ST5 isolates and 3 non-ST5 isolates,

756 total N=40 mice in each experiment). All mice were sacrificed at day 7 post-infection in the first experiment and at day 14 post-infection in the
757 second experiment to assess *in vivo* fungal burden in mouse lung and brain. Fungal burden in the lung and brain at either day 7 or day 14 for
758 each isolate is presented in panel A. In the last experiment, ten A/J mice were infected with each of the 8 test *C. neoformans* isolate (five ST5
759 isolates and 3 non-ST5 isolates, N=80 mice in total) and monitored daily until the point when 15% of body weight loss, a sign of distress and
760 impending death, was evident. Fungal burden in lung and brain at point of death was again assessed as before. Here, for each strain, five mice
761 were randomly selected from the ten test mice for fungal burden investigation. The pooled fungal burden in non-ST5 infections was higher than
762 in ST5 infections in both lung tissue at all time points, and in brain tissue at the point of sacrifice (Panel B) (For P values see text). Boxplots
763 (Tukey's method) describe the median and interquartile range, the whiskers demarcate the largest or smallest values that were not outliers
764 (black dots); outliers are defined as more than 1.5 times the interquartile range from the nearest quartile.



765

766

767 **Figure 4. Genotype-specific cytokine concentrations from lung homogenate of A/J mice at 7 and 14 days post infection with 5×10^4 *C.***

768 ***neoformans* cells/mouse.** Five mice were infected with each strain from each genotype at each time points. ST5 strains induced significantly

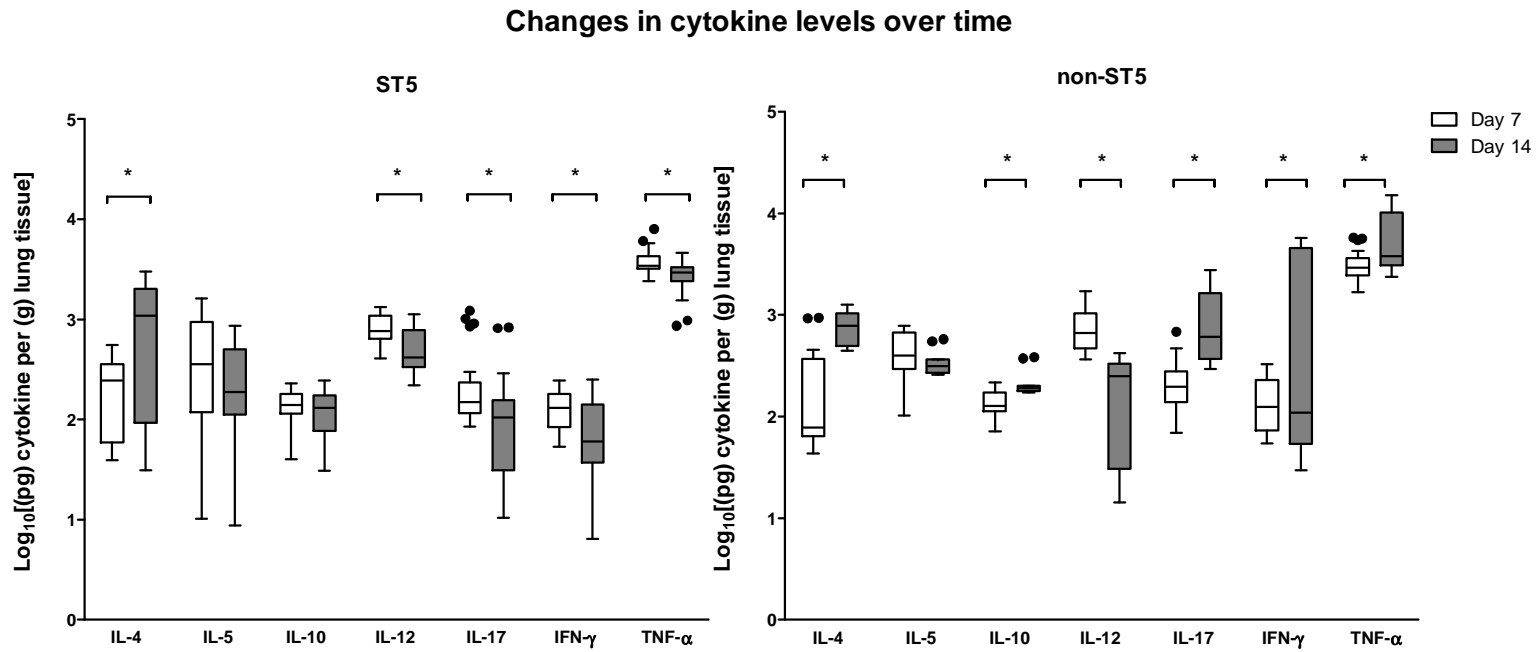
769 higher levels of TNF- α at day 7, suggesting an earlier and more profound initial inflammatory response in infected mice. By day 14 mice infected

770 with non-ST5 strains have higher levels proinflammatory cytokines, probably a result of ST5 yeasts being cleared more rapidly from infected

771 mice. The horizontal line within the box indicates the median; boundaries of the box indicate the 25th and 75th percentile and the whiskers

772 indicate the highest and lowest values of the results; outliers are denoted as black dots (Tukey's method). Data are standardized as picograms of
773 cytokine per gram lung tissue. Asterisks indicate statistically significant differences (Mann-Whitney test).

774



775

776 **Figure 5. Genotype-specific changes in cytokine concentrations from lung homogenate of A/J mice infected with *C. neoformans* between day**
777 **7 and day 14 post-infection.** Box and whisker plots (Tukey's method) compare levels of each cytokine between day 7 and day 14 for each
778 genotype. Data are standardized as picograms of cytokine per gram lung tissue. Asterisks indicate statistically significant differences (Mann-
779 Whitney test).

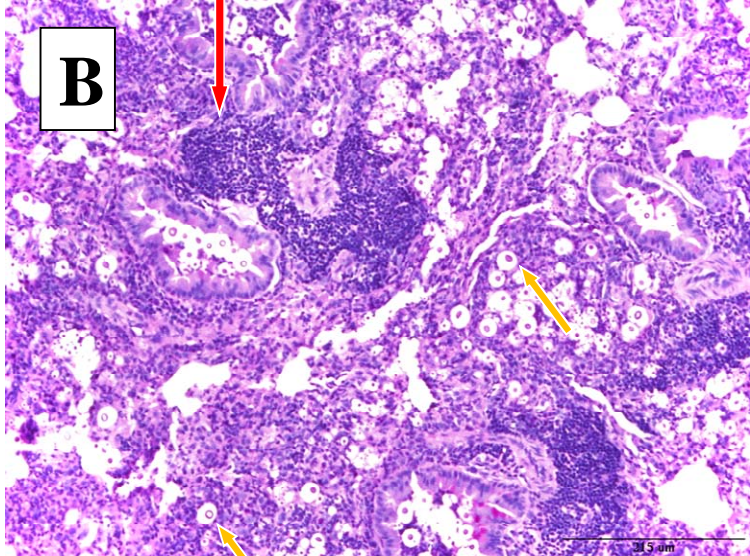
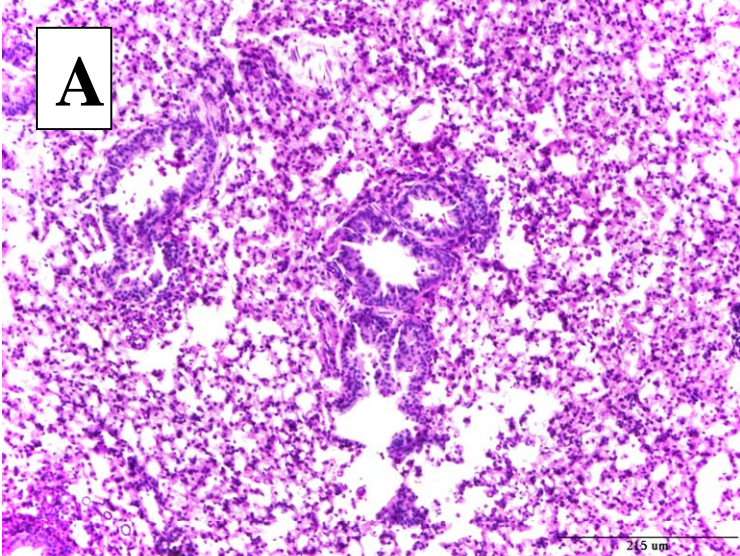
780

781

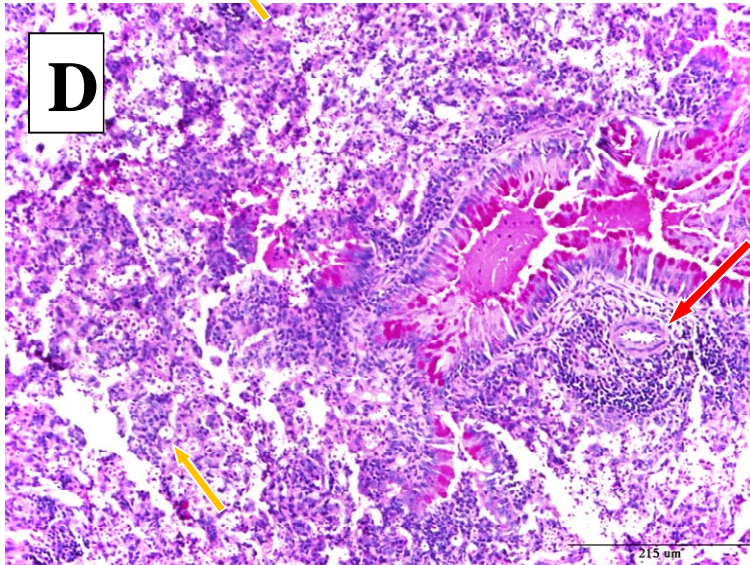
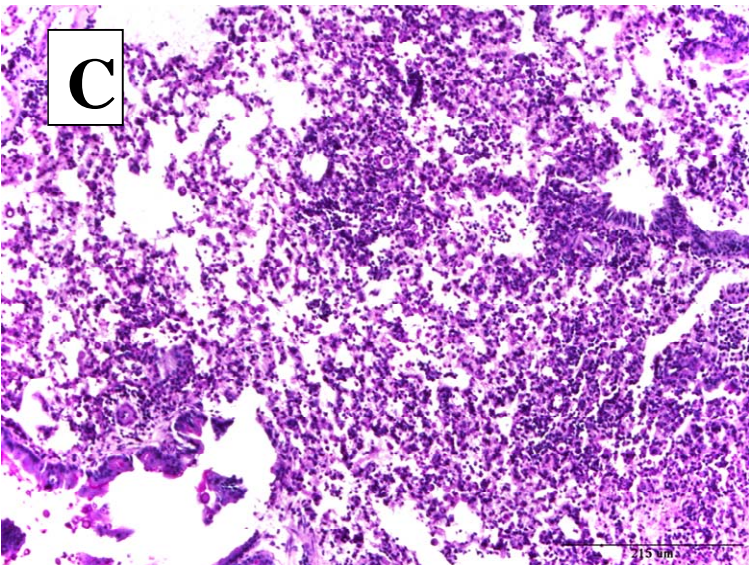
Day 7

Day 14

BMD1338
VNI- γ /ST5



BMD1415
VNI- δ /ST4



783 **Figure 6. Periodic Acid Schiff (PAS) staining of pulmonary tissue from mice infected with BMD1338 and BMD1415 on days 7 and 14.** The two
784 strains represent ST5 and non-ST5, respectively. A/J mice were inoculated intranasally with 5×10^4 yeast cells. Lung specimens were harvested at
785 days 7 and 14 for histopathological examination. Photomicrographs were obtained at 200X magnification; the scale bar represents 215 μm). (A-
786 B): lung sections from mice infected with BMD1338 (VNI- γ /ST5) at day 7 and day 14, respectively. (C-D): lung sections from mice infected with
787 BMD1415 (VNI- δ /ST4) at day 7 and day 14, respectively. Perivascular infiltration (red arrows) and necrosis are more marked by day 14 for both
788 strains. Encapsulated yeasts (yellow arrows), notable for the larger cell size and capsule thickness of BMD 1338 compared with BMD1415.

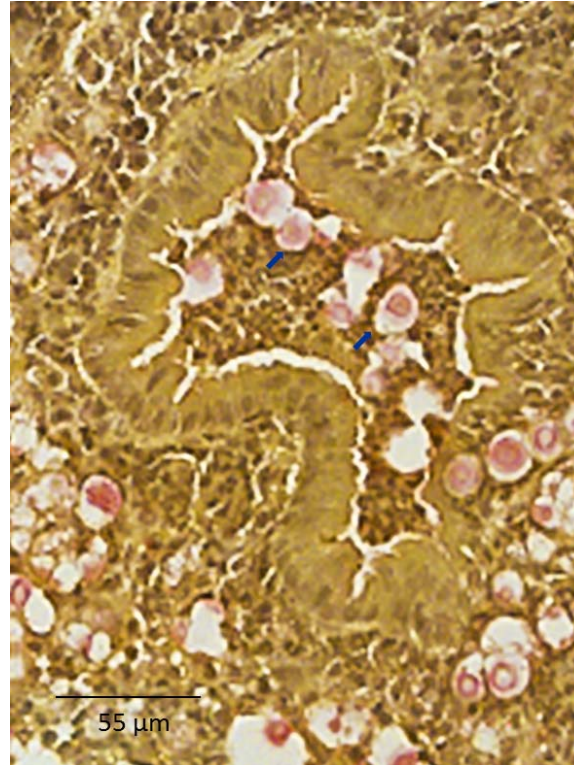
789

790

791

792

793



794

795 **Figure 7. Mucicarmine staining of capsular material in paraffin-embedded mice pulmonary tissue.**

796 Uninflated lung specimens were harvested from mice as described in the methods. Mucicarmine staining was performed to visualize the
797 cryptococcal capsule. Photomicrographs were captured at 400X magnification with scale bar indicating 55μm. Capsular polysaccharide is stained
798 pink (indicated by blue arrows), demonstrating diffuse localization consistent with extensive capsule production by yeasts in the alveolar space.

799

